Article

Thermal Decomposition and Solidification Characteristics of BFFO

Yiming Luo [1,2], Ronghui Ju [2,3], Bingbo Li [2], Junjiong Meng [2] and Xuanjun Wang [1,4],*

1   High-Tech Institute of Xi'an, Xi'an 710025, China; iamrlym@126.com
2   Xi'an Modern Chemistry Research Institute, Xi'an 710065, China; ronghuiju@126.com (R.J.);
    lbb500@sina.com (B.L.); mengjunjiong204@163.com (J.M.)
3   Beijing Institute of Technology, School of Chemistry and Chemical Engineering, Beijing 100081, China
4   Zhijian Laboratory, Xi'an 710025, China
*   Correspondence: wangxj503@sina.com

Abstract: A novel energetic material, Bifurazano [3,4-b: 3',4'-f] furoxano [3'',4''-d] oxacyclo-heptatriene (BFFO), has been investigated regarding two aspects, namely its thermal decomposition and solidification characteristics. The DSC curves indicate that the peak temperature of BFFO decomposition process is 271.1 °C under the static pressure of 2 MPa and the volatility of BFFO at 120 °C is significantly lower than that of TNT, DNAN and DNTF. The solidification curve indicates that the solidification of BFFO is a basic linear uniform solidification process, which is obviously different from that of TNT, DNAN and DNTF. In addition, the facet of BFFO appears much smoother and fewer defects are observed in the solidified body after solidification via CT and SEM. The reduction in solidification defects also further improves the mechanical properties of BFFO, with significant improvements in compressive and tensile strength compared to DNTF, DNAN and TNT. In summary, BFFO is a potential melt-cast carrier explosive with excellent thermal stability, solidification characteristics and mechanical properties.

Keywords: BFFO; thermal decomposition; solidification characteristics; solidification defect; layer by layer solidification; solidification rate

1. Introduction

High energy density materials (HEDMs) with excellent detonation properties have been at the forefront of energetic materials research. In particular, the development of insensitive high-energy-density melt-castable explosives has received increased attention from the scientific and engineering community over past few decades. In general, a melt-castable material should have a melting point between 70 and 120 °C, preferably below 100 °C. This allows heating steam to be used at ambient pressures in casting operations, which can dramatically reduce costs in manufacturing. In addition, a significant separation between the melting point and the decomposition temperature is ideal. Meanwhile, such a material must also possess other meaningful specific unique properties, including high loading density, low vapor pressure, low sensitivity, low toxic, and green and affordable preparation [1].

To date, the most widely used melt-cast explosive has been 2,4,6-trinitrotoluene (TNT), due to its favorable comprehensive performance as both a military and industrial explosive [2]. However, research has found that long-term exposure to TNT may result in critical health risks [3]. Firstly, TNT can cause hemolytic anemia and aplastic anemia. Secondly, the liver damage caused by TNT mainly affects the detoxification function, excretion function and sugar metabolism of the liver. In addition, TNT can cause local or global lesions in the lens and, in severe cases, can form cataracts.

TNT suffers from relatively high vapor pressure, undergoes photolysis degradation easily and is sensitive to reactions in alkaline environments [4]. Waste, especially red

water and pink water, generated during the TNT manufacturing process can cause serious environmental pollution [5]. Red water is the waste generated during the TNT purification process. It is characterized by its alkaline pH of 8 and is composed of a complex mixture of nitroaromatic hydrocarbons and inorganic salts. Pink water is the washing water generated during the precision processing of TNT, in which TNT is dried, flaked and packaged. Pink water is typically saturated with an amount of TNT that dissolves in water and is produced as a result of equipment washing processes following demilitarization or munition-filling operations. The US Environmental Protection Agency has declared TNT as a pollutant and has promoted its removal from military ammunition [6]. Due to its environmentally problematic and toxic to human health characteristics, TNT has gradually fallen out of favor in the field of energetic materials.

2,4-Dinitroanisole (DNAN), one of the early candidates for TNT replacement, was originally selected due to a shortage of TNT in World War II, rather than the concern about the sensitivity of munitions [7], although it is insensitive to external stimuli. However, DNAN has a low density of 1.544 g cm^{-3} and a detonation velocity of 5974 m s^{-1} [8], making it difficult to replace the status of TNT(density of 1.654 g cm^{-3} and a detonation velocity of 6970 m s^{-1}) in the family of energetic materials. Therefore, there is increasing interest in developing a melt-castable material that is more powerful and less toxic than TNT.

As important components in the development of HEDMs, energetic furazan and furoxan compounds feature high density and active oxygen, high formation heat and good thermal stability [9–15]. Of these, the castable multi-furazan cyclic compounds represented by 3,4-bis(3-nitrofurazan-4-yl) furoxan (DNTF) have been of practical value, as they display a high detonation velocity (D = 9250 m·s^{-1}), high density (ρ = 1.937 g·cm^{-3}) and low melting point (T$_m$ = 110 °C). Additionally, the thermal stability of DNTF is quite high: a 5 s delay exploding point is 308 °C [16–19]. However, the practical application of these materials is still limited by the high impact sensitivity.

Recently, furazan ether compounds have drawn much interest from scientists. Energetic structural units, such as furazan and furoxan, are able to significantly increase the energy density of the compound and improve the oxygen balance. At the same time, the introduction of ether bonds significantly increase the molecular flexibility, providing the compounds with plastic strength and low sensitivity, combined with energy, safety and mechanical properties. One of these compounds, bifurazano [3,4-b: 3′,4′-f] furoxano [3″,4″-d]oxacycloheptatriene (BFFO), with two furazan and one furoxan cycles fused into the oxacycloheptane ring, is expected to be an excellent melt-cast carrier explosive [20–22]. Its molecular structure is shown as Figure 1 and the energy properties are listed in Table 1 [23].
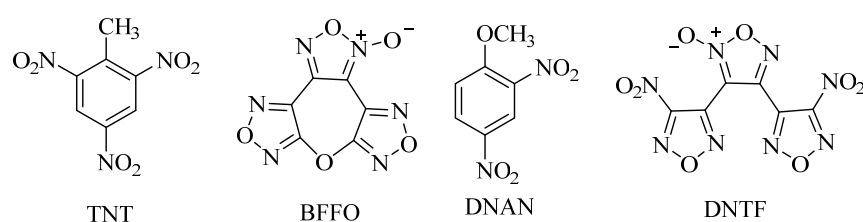

Figure 1. Molecular structures of TNT, DNAN, DNTF and BFFO.

Table 1. The energetic properties of BFFO.

T_m (°C)	ρ (g·cm^{-3})	IS (%) [1]	FS (%) [2]	H_{50} (cm) [3]	D (m·s^{-1}) [4]	Q_V (J·g^{-1}) [5]
92–94	1.870	12	0	57.5	8256	6162

[1] Impact sensitivity; [2] friction sensitivity; [3] the 50% critical drop height of detonation; [4] detonation velocity; [5] heat of detonation.

To date, very little attention has been paid to the melt-cast process property of BFFO, despite its known relevant, significant energetic characteristics. This paper investigates BFFO regarding several aspects, including thermal decomposition and solidification char-

acteristics. Meanwhile, widely used melt-cast carrier explosives, namely TNT, DNAN and DNTF, were chosen as comparisons.

2. Experimental Details

2.1. Materials

BFFO, DNTF, DNAN and TNT were synthesized in the Xi'an Modern Chemistry Research Institute. The purity of four energetic materials was above 99%, analyzed via high-performance liquid chromatography.

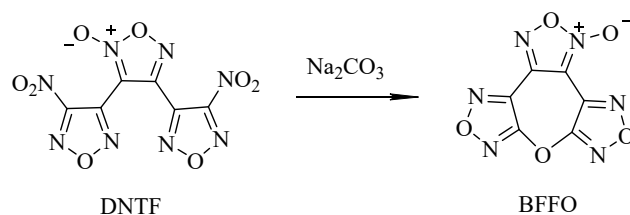BFFO was obtained from DNTF through etherification at a yield of 50.1%, as shown in Figure 2 [23].

Figure 2. Synthesis route of TFO.

Powder X-ray diffraction (PXRD) data of BFFO, as shown in Figure 3, were collected at room temperature on a Rigaku Ultima IV X-ray diffractometer (CuKα radiateon, 40 kV tube voltage, 44 mA current). The 2θ range measured was 5–60° with steps of 0.02°/0.1 s.
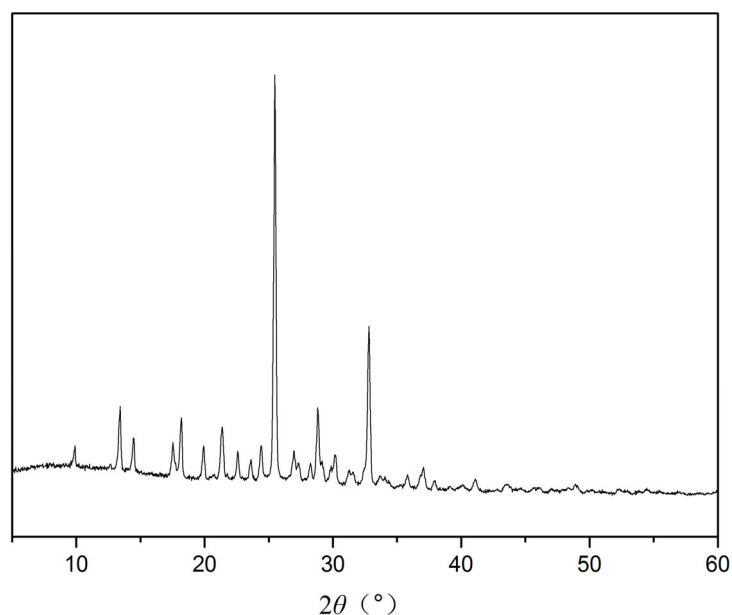

Figure 3. XRD curve of BFFO.

2.2. Thermal Analysis (TA)

Thermal analysis (TA) comprises a family of measuring techniques that share a common feature: they measure the response of a material to being heated or cooled (or, in some cases, held isothermally).

Thermal analysis includes a series of measurement techniques with common characteristics, which mainly measure the response of materials to being heated, cooled or held isothermally, in some cases. The most commonly used techniques are differential scanning calorimetry (DSC) and thermogravimetry (TG). In this study, the thermal decomposition characteristics of BFFO under high pressure were studied via a pressure differential scanning calorimetry (PDSC, NETZSCH, DSC 204 HP) and compared with those of other carrier explosives. The sample, with a mass of 1.00 ± 0.01 mg, was heated from 30 °C to 400 °C

under a dynamic nitrogen atmosphere of 50 mL·min^{-1} and was tested under atmospheric pressure of 2 MPa, respectively.

TG under a nitrogen atmosphere was conducted on a METTLER TOLEDO TGA/DSC apparatus at a constant temperature (120 °C for 4 h) under flowing nitrogen atmosphere (20 mL·min^{-1}) in open platinum crucibles. As the size of the sample pan in the instrument was very small, only 3–5 mg samples were used in the experiments. The reference material was an empty Al$_2$O$_3$ crucible. With the help of simultaneous thermal analyzer, the data of DSC and TG were obtained simultaneously.

2.3. Solidification Characteristics

2.3.1. Solidification Temperature Curve Test

In order to investigate the solidification characteristics of BFFO, an experimental facility was established, as shown in Figure 4. The facility consisted primarily of a thermocouple temperature measurement system and a mold in which the molten explosive was solidified. The height of the mold was 200 mm, and the radius of the mold was 60 mm. The thermocouple probe was located at the center of the cylinder and selected as the point of measurement due to this location being the typical region in which porosity often developed. The experimental procedures are described as follows: (1) The molten BFFO explosive was prepared and maintained at 95 °C. (2) The molten explosive was poured into the mold and began solidification, while the thermocouple measurement system recorded the temperature–time course at the measurement point until the temperature decreased to 20 °C. The heights of the sensors were 30 mm (1#), 70 mm (2#), 110 mm (3#) and 150 mm (4#) from the bottom of the mold.
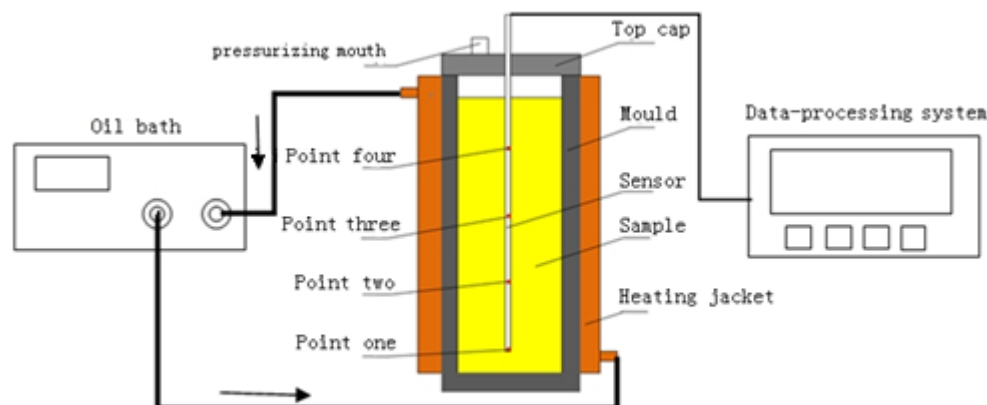

Figure 4. Schematic diagram of solidification rate test device.

2.3.2. Programmed Solidification Test

A METTLER TOLEDO TGA/DSC 3+ machine was used to test the solidification process of BFFO. The atmosphere was dynamic high purity nitrogen, and the flow rate was 50 mL·min^{-1}. The melting section was heated to 110 °C at a rate of 10 °C·min^{-1}, and the solidification section was cooled to 20 °C at a rate of -1 °C·min^{-1}. The sample dish was an aluminum pool opening, and the sample was 10 mg.

2.3.3. Solidification Defects Characterization

The distribution of solidification defects was an important factor that affected the quality control of the casting charge. The more concentrated the solidification defects are, the easier it is to control the charging quality. In order to understand the macroscopic distribution of solidification defects of melt-cast explosives, industrial computerized tomography (industrial CT) was used for the nondestructive inspection of the solidification defects. The explosive samples were positioned on the deck between the source and detector. By rotating the deck, the X-ray detector can clearly observe the internal defects of the sample.A series of preliminary imaging experiments were conducted on typical samples using different

combinations of scanner settings. The voxel size of the sample related to two parameters: distance from the sample to the source and from the detector to the source. The voltage and current of the tube were 90 kV and 90 mA, and the magnification factor was 44.87.

2.3.4. Mechanical Property Test

The mechanical properties of the solidified sample were tested. The mechanical properties of explosives were characterized by compressive strength and tensile strength. For the tensile strength test, the sample was Ø20 × 20 mm, and for the compressive strength test, the column sample was Ø20 × 20 mm. All samples were tested at a nominal loading rate of 0.5 mm·min^{-1}.

3. Results and Discussion

3.1. Thermal Behavior

3.1.1. Thermal Decomposition Study by DSC

The thermal analysis (DSC) of BFFO, TNT, DNAN and DNTF under air atmosphere with a heating rate of 10 °C·min^{-1} is shown in Figure 5. It was found that BFFO had a distinct endothermic melting process with a peak temperature at 231.2 °C due to its strong volatility at a heating rate of 10 °C·min^{-1} under atmospheric pressure. A similar feature also appeared in the DSC curve of TNT, DNAN and DNTF, whose endothermic peak temperatures appeared at 236.2 °C, 259.7 °C and 231.2 °C, respectively.
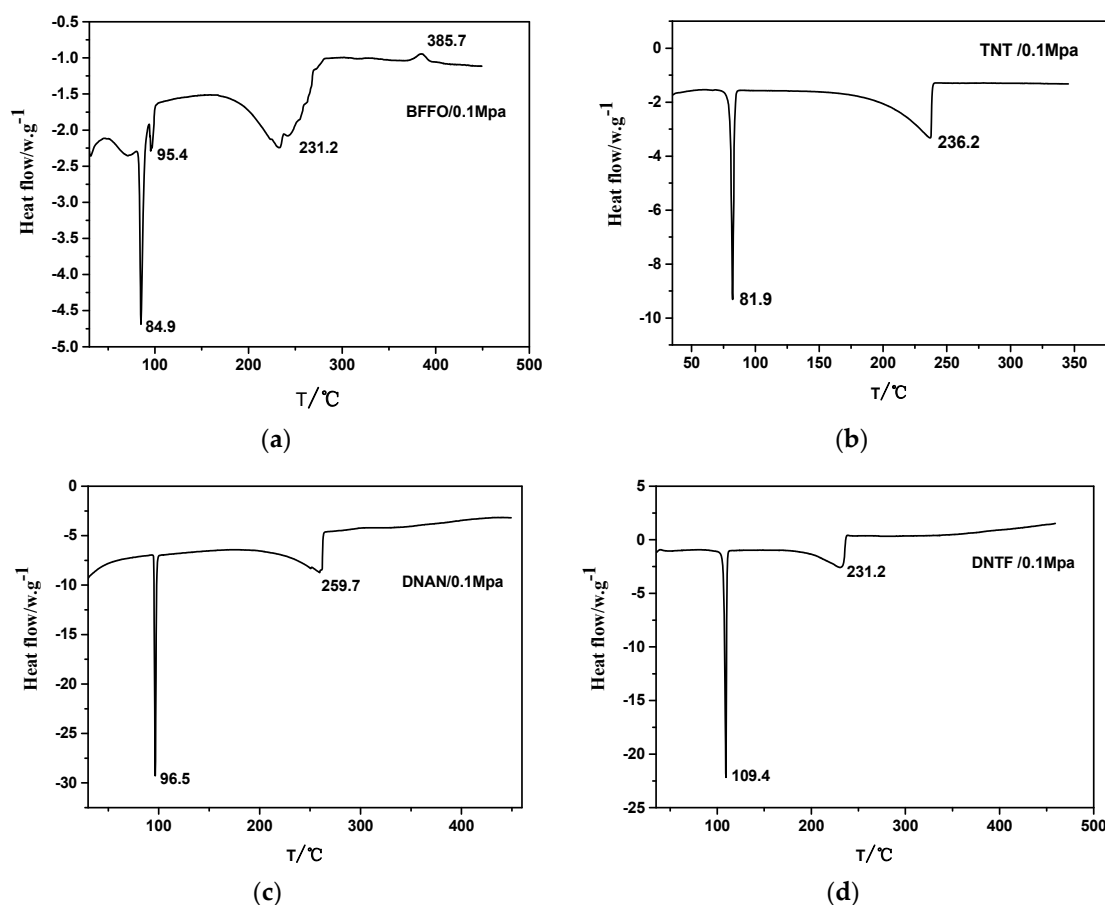

Figure 5. DSC curves of BFFO, TNT, DNAN and DNTF under atmospheric pressure: (**a**) BFFO; (**b**) TNT; (**c**) DNAN; (**d**) DNTF.

When the samples were subjected to the static pressure of 2 MPa, by contrast, the BFFO, TNT and DNTF all exhibited intense exothermic decomposition processes with the peak temperatures of the decomposition process located at 271.1 °C, 308.2 °C and 274.4 °C, respectively. DNAN, however, still exhibited no exact exothermic decomposition peaks (Figure 6).
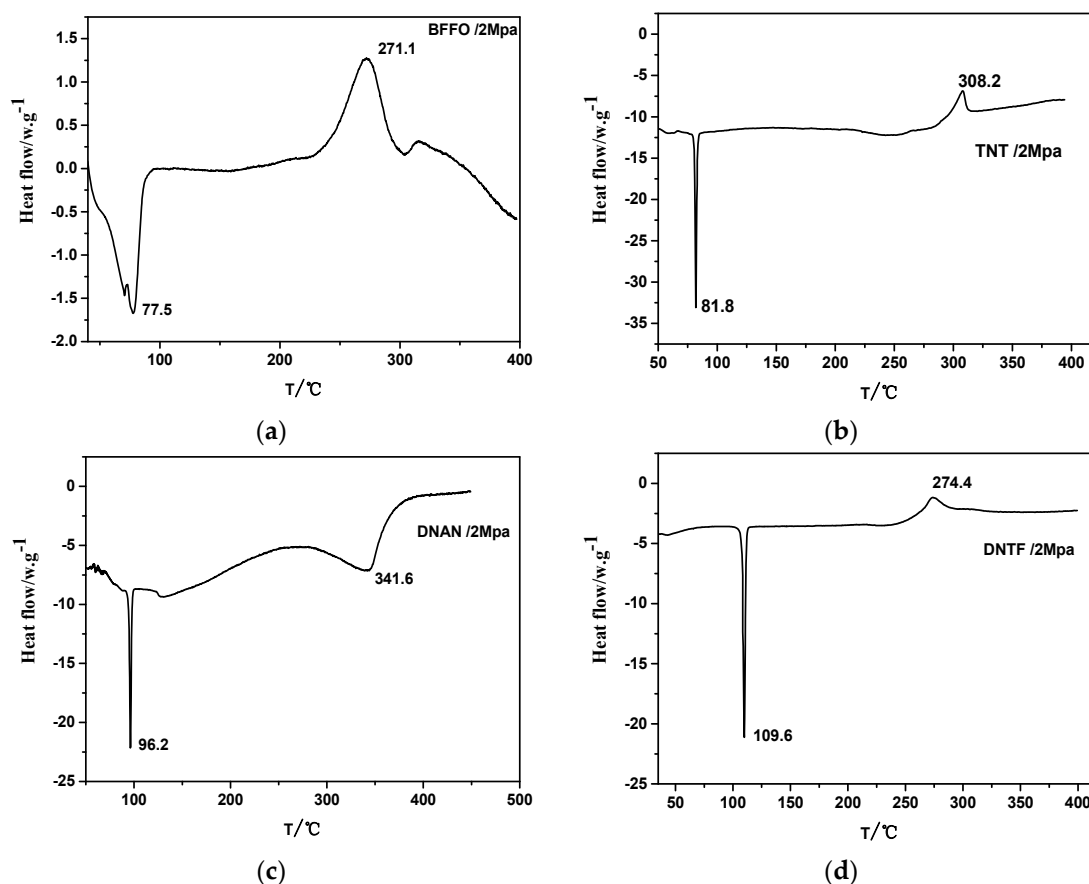
Figure 6. DSC curves of BFFO, TNT, DNAN and DNTF at 2 Mpa: (**a**) BFFO; (**b**) TNT; (**c**) DNAN; (**d**) DNTF.

3.1.2. Volatility under Isothermal Conditions

The volatility of BFFO at a casting temperature of 120 °C was investigated and compared with other common melt-cast explosives. As revealed by the isothermal TG curve (Figure 7), the volatility of BFFO at 120 °C was significantly lower than that of TNT, DNAN and DNTF. The data were further linearly fitted in Table 2 and exhibited the volatilization rates of BFFO, TNT, DNAN and DNTF, which are 3.31%·h^{-1}, 8.07%·h^{-1}, 5.29%·h^{-1} and 7.61%·h^{-1}, respectively, indicating that BFFO could be a promising melt-cast carrier explosive in terms of volatility.
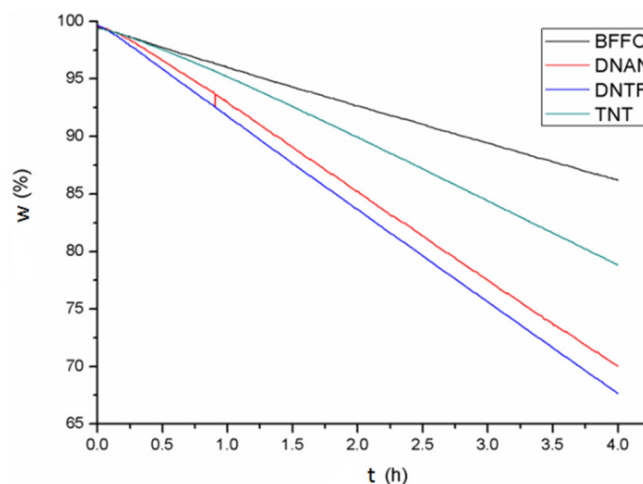

Figure 7. The isothermal TG curve of BFFO, TNT, DNAN and DNTF at 120 °C.

Table 2. The fitting equations and related parameters of the isothermal TG curves of BFFO, TNT, DNAN and DNTF at 120 °C.

Sample	Fitting Equations	R [1]
BFFO	y = −3.31446x + 99.34044	0.99968
TNT	y = −5.29571x + 10028905	0.99862
DNAN	y = −7.60659x + 100.37098	0.99975
DNTF	y = −80.07014x + 99.82379	0.99996

[1] The correlation coefficient.

3.1.3. Calculation of BFFO Thermal Explosion Temperature

The heat preservation and care process after the slurry is cast is an important process during the preparation of melt-cast explosives. Depending on the amount of explosive and the projectile body, this process can last for several hours. During this process, the accumulation of heat can lead to a slow decomposition of the substance, which can cause intense reactions. This issue is referred to as thermal stability when the heating rate reaches zero. The general formula for the mechanism function of the thermal decomposition reaction of explosives is as follows:

$$f(\alpha) = (1 - \alpha)^n \tag{1}$$

where a is the decomposition fraction of the explosive and n is the reaction order, which is related to the specific material properties. Based on the thermal decomposition data of BFFO in Figure 6a, combined with the most probable mechanism function judgment method, the universal integration method of Equation (2) was used to solve various mechanism functions, and the average activation energy Ea of BFFO was 129.47 kJ·mol^{-1}.

$$ln\left[\frac{G(\alpha)}{T - T_0}\right] = ln\frac{A}{\beta} - \frac{E}{RT} \tag{2}$$

where $G(a)$ is the integral form of the mechanism function; T is the temperature corresponding to different reaction depths, K; T_0 is the initial reaction temperature, K; β is the heating rate, K·min^{-1}; A is the pre-exponential factor; E is the reaction activation energy, kJ·mol^{-1}; and R is the gas constant.

The Zhang–Hu–Xie–Li Method for predicting the critical temperature of a thermal explosion from thermal decomposition curves is as follows:

$$T_b = \frac{E - \sqrt{E^2 - 4ERT_{e0}}}{2R} \tag{3}$$

where T_b is the thermal explosion critical temperature of the energetic material when $\beta \to 0$, K.

The thermal explosion critical temperature (T_b) of BFFO is 270.8 °C which is calculated from formula 3, indicating that BFFO possesses good thermal stability generally and thermal stability as a melt-cast carrier explosive.

3.2. Solidification Characteristics Study

3.2.1. Solidification Temperature Curve Test

The solidification temperature curves of TNT, DNAN, DNTF and BFFO are shown in Figure 8 [24,25]. The solidification processes of TNT, DNAN and DNTF exhibited typical crystal solidification characteristics. To be specific, the samples started to solidify when the temperature reached the freezing point, and the temperature remained unchanged during solidification. Then, after the complete solidification of the samples, the temperature began to drop.
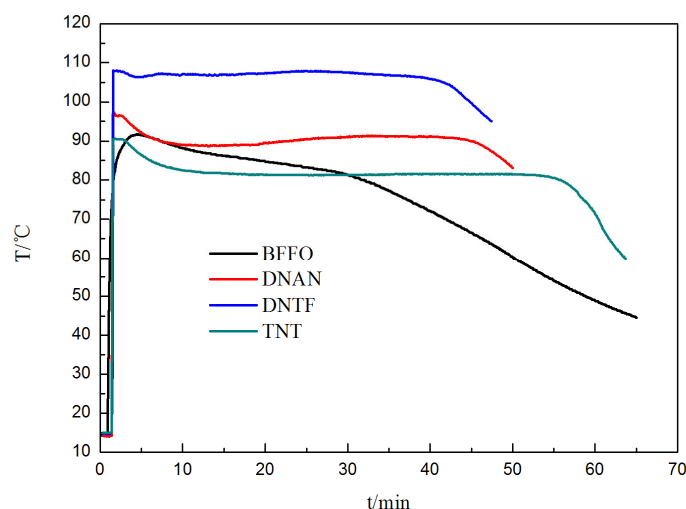
Figure 8. Solidification temperature curves of TNT, DNAN, DNTF and BFFO.

The solidification time of TNT was longer than that of DNAN and TNTF, which may be due to the lower solidification point of TNT and the smaller temperature difference between the sample and the environment.

In the constant temperature section at the freezing point of the cooling curve, the temperature of TNT was relatively stable, while the temperature of DNTF fluctuated, which may have been due to the low thermal conductivity of DNTF. The DNTF near the solidification layer was re-heated by the latent heat of crystallization, and the heat received was difficult to export. At the same time, the low specific heat capacity led to a temperature change caused by a small amount of accumulated heat, resulting in a small fluctuation of temperature. In addition, the solidification characteristics that DNAN exhibited were similar to those of DNTF, except that the solidification temperature and solidification time were different.

The solidification curve of BFFO was obviously different from those of TNT, DNAN and DNTF. To be specific, the solidification process of BFFO exhibited a basic linear uniform solidification process rather than a clear platform, showing brand new solidification characteristics. In fact, the solidification of BFFO is a process of transitioning from liquidity to amorphous materials, and BFFO molecules do not crystallize during the cooling process as TNT, DNAN and DNTF do. It should be noted that BFFO and DNTF have similar molecular structures, but they show different solidification and crystallization characteristics during solidification. The dynamic process of amorphous formation requires overcoming potential barriers, and the transition from liquid state (with small particle flow barriers) to amorphous solid state (with large particle flow barriers) is mainly due to changes in its flow barriers. The rheological barrier is mainly determined by the chemical bond properties of the material. In BFFO molecules, ether bonds connect two furazan groups to form a cyclic structure. This structure leads to a high viscosity in the liquid, forming a large crystalline barrier, which is not conducive to the long-range ordered arrangement of BFFO molecules, leading to the formation of amorphous materials.

3.2.2. Programmed Solidification Test

Further solidification tests were conducted on BFFO and DNTF through DSC, and the solidification curves are shown in Figure 9.

As shown in Figure 9, a cooling rate of $1\ °C \cdot min^{-1}$ was used to control the solidification of BFFO. When the temperature was lowered to 20 °C, no clear solidification crystallization peak for BFFO was observed. However, DNTF began to solidify at 45.5 °C with a latent heat peak at 44.7 °C, and the solidification was completed at 43.6 °C. DNTF formed a sharp solidification peak with a solidification temperature span of 0.9 °C, indicating that the solidification process of DNTF triggered by supercooling was a rapid crystallization process.
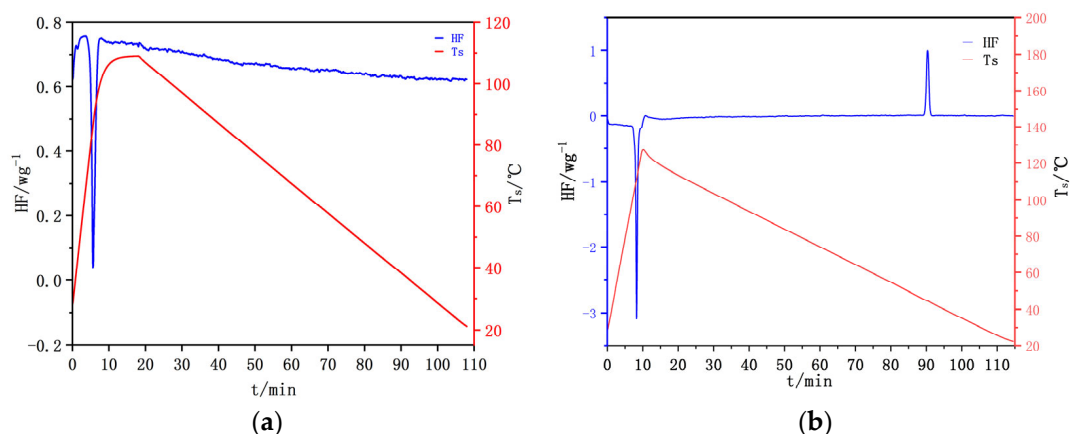
Figure 9. DSC solidification Curves of BFFO and DNTF: (**a**) BFFO; (**b**) DNTF.

Further macroscopic solidification experiments were conducted on BFFO, and it was found that the solidification of BFFO was a very slow crystallization process. As shown in Figure 10, BFFO maintained a molten state for a long time, then slowly nucleated, solidified, and completed solidification after about 55 h. This characteristic was significantly different from the solidification characteristics of typical melt-cast explosives, such as TNT and DNTF, indicating that further research on this characteristic is necessary.

Figure 10. Solidification characteristics of BFFO.

3.2.3. Solidification Defects Study

In this paper, BFFO, TNT, DNAN and DNTF columns at a size of Ø 60 mm × 100 mm were cast, and the internal defects of the columns after natural cooling are shown in Figure 11. The volume shrinkage of TNT was obvious, and the solidification process was accompanied by a phenomenon of self-aggregation. Obvious solid phase aggregation and contraction voids were observed at the same time. When BFFO solidified, the pores gradually gathered in the top area and a pore structure with large shrinkage was formed. No penetrating shrinkage structure from bottom to top at the central axis of charge was observed. TNT, DNTF and DNAN, by contrast, displayed penetrating shrinkage structures. The test results indicated that the quality of the BFFO casting charge was significantly better than those of DNTF, DNAN and TNT, and no internal shrinkage existed.

In addition, BFFO and three other melt-cast explosives were characterized via the examination of their surface and morphological features using SEM, and the results are shown in Figure 12. Although only limited characterization analyses have been performed so far, several obvious differences and similarities between these explosives have been observed.

Compared with other carrier explosives, BFFO possesses smoother facets, a neatly arranged crystal structure and fewer defects, which may benefit from the relatively linear solidification characteristic of BFFO. To be specific, such solidification characteristic provided a very favorable condition for the generation of dense and small grains during the solidification process of BFFO, thereby significantly reducing the shrinkage cavity, shrinkage porosity and other defects of the whole casting. The irregularities appeared on the facets of DNAN, and no obvious volume shrinkage was observed. Many shrinkage

defects were scattered in the solidified charge, which differed from the microstructure of TNT crystals significantly.
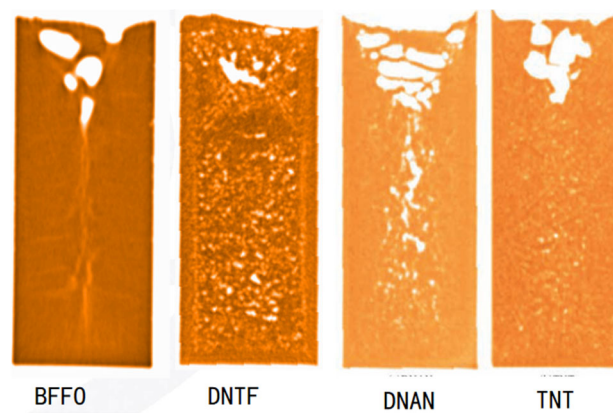

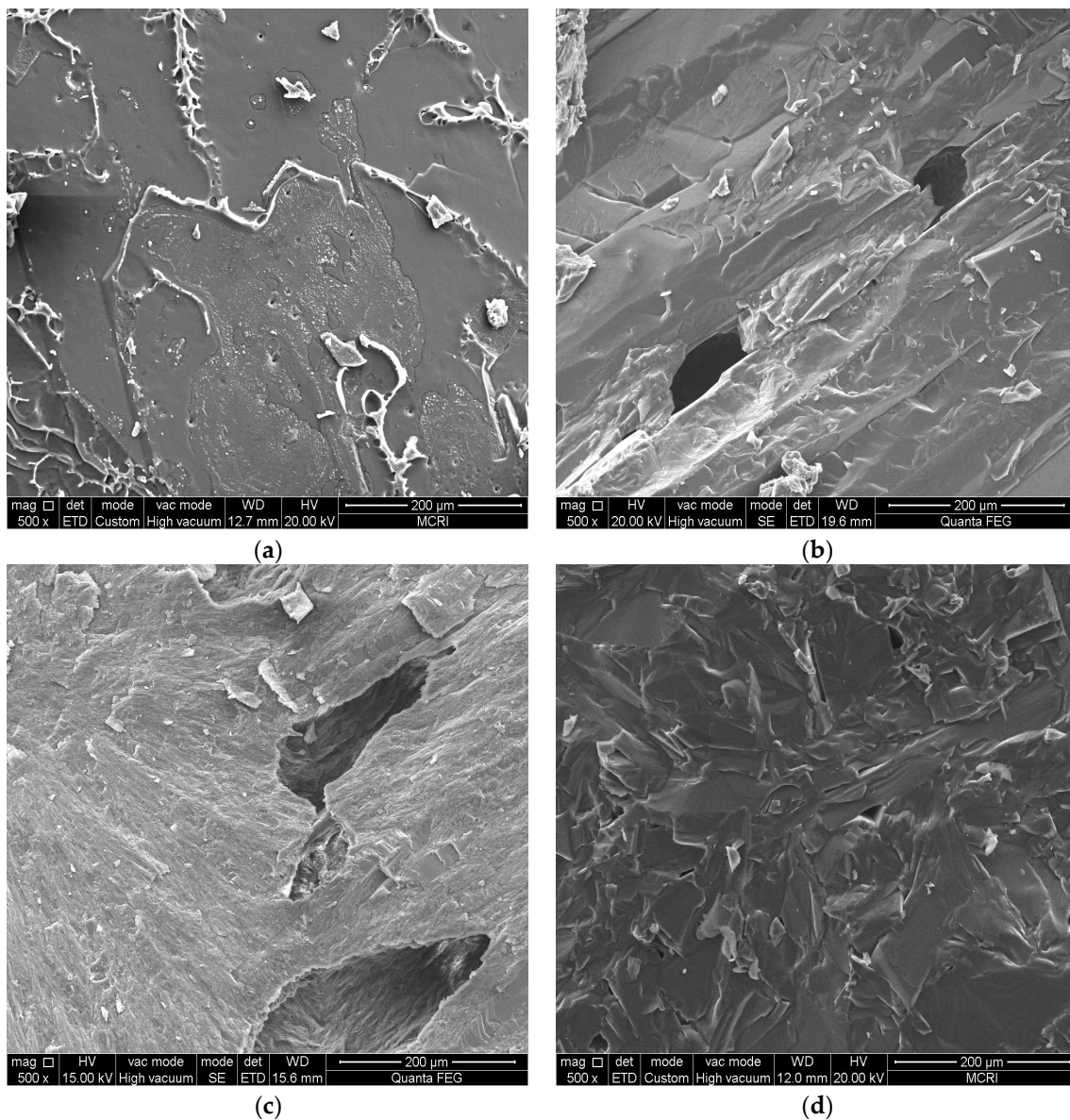**Figure 11.** The distribution of solidification defects.

Figure 12. SEM pictures of BFFO, TNT, DNAN and DNTF: (**a**) BFFO; (**b**) DNTF; (**c**) DNAN; (**d**) TNT.

3.2.4. Mechanical Property Test

As a brittle material, melt-cast explosives are prone to fracturing during long-term utilization and storage, which affects the safety of ammunition. Therefore, the improvement of mechanical properties is one of the focuses of research on melt-cast explosives. The mechanical properties of BFFO, DNTF, DNAN and TNT were tested using a mechanical property testing machine, and the test results are shown in Table 3.

Table 3. The mechanical properties of BFFO, DNTF, DNAN and TNT.

EMs	$\Phi \times h$ (mm)	Density ($g \cdot cm^{-3}$)	Compressive Strength (Mpa)	Tensile Strength (Mpa)
BFFO	20×20	1.774	6.07	2.44
DNTF	20×20	1.687	3.24	1.25
DNAN	20×20	1.514	2.67	1.32
TNT	20×20	1.573	3.88	1.77

As shown in Table 3, the compressive strength and tensile strength of BFFO was significantly higher than those of DNTF, DNAN and TNT. To be specific, the compressive strengths were 87.3%, 127.3% and 56.4% higher than those of DNTF, DNAN and TNT, respectively. The tensile strengths were 95.2%, 84.8% and 37.9% higher than those of DNTF, DNAN and TNT, respectively. The analysis revealed that, on the one hand, the introduction of ether bonds into the molecules of BFFO significantly increased the flexibility of the material and improved its mechanical properties. On the other hand, good solidification molding performance reduced micro defects during BFFO castings, thereby further improving mechanical properties.

3.2.5. Analysis of Solidification and Crystallization Behavior

The solidification could be classified as layer-by-layer solidification, volumetric solidification and mid-solidification, according to the solidification theory. The characteristics are as follows [26]:

- The width of solidification zone during layer-by-layer solidification is very narrow, and the front is in direct contact with the melt. The volume shrinkage occurs when the liquid phase solidifies into solid phase, and the melt can be replenished continuously, leading to very small possibility of dispersed shrinkage in the casting. A concentrated shrinkage cavity will be left at the final solidified part. In this case, the feeder can be used to eliminate the defects inside the casting.
- The solidification zone of volumetric solidification is wide, and it can easily develop into a dendritic structure with developed dendritic crystals. When these dendrites are connected to each other, the unsolidified melt is divided into disconnected melt pools, and dispersed shrinkage cavities are finally formed in the casting. It is difficult to eliminate the internal defects of such castings via feeders.
- Mid-solidification is a solidification form between layer-by-layer solidification and volumetric solidification.

Regarding the distribution of macroscopic and microscopic defects and temperature–time curves in the solidification process, the four melt-cast explosives exhibited different solidification behaviors. To be specific, TNT tended to display layer-by-layer solidification and DNTF tended to display volumetric solidification. DNAN belonged to the mid-solidification. Compared with the above processes, BFFO exhibited a very typical layer-by-layer solidification process, which was mainly caused by the lower solidification rate of the melt. When the BFFO melt at the solid–liquid interface was solidified and crystallized, a certain degree of volume shrinkage occurred, resulting in micro-defects appearing near the solidified solid phase. Due to the low solidification rate of BFFO, the solid–liquid interface moves slowly, and the BFFO melt in the previous section has sufficient time to fill the pore defects in the next section. This phenomenon occurs repeatedly during the

solidification process of the BFFO melt until the melt is completely solidified. Therefore, the solidified crystalline structure of BFFO has fewer micro defects, and a typical funnel-shaped shrinkage cavity was generated at the macro level. Benefiting from the reduction in micro defects, BFFO possessed higher mechanical strength in terms of mechanical properties.

4. Conclusions

In this study, several aspects of Bifurazano [3,4-b: 3′,4′-f] furoxano [3″,4″-d] oxacyclo-heptatriene (BFFO) were studied, including thermal decomposition and solidification characteristics, and widely used melt-cast explosives, namely TNT, DNAN and DNTF, were chosen for comparison. The following conclusions were reached:

1. The DSC curves indicate that the peak temperature of the BFFO decomposition process was 271.1 °C under a static pressure of 2 MPa and the volatility of BFFO at 120 °C was significantly lower than those of TNT, DNAN and DNTF.
2. The solidification curve indicated that the solidification process of BFFO exhibited a basic linear uniform solidification process, which was obviously different from the clear platform of TNT, DNAN and DNTF.
3. The results of the CT defects indicate that the facet of BFFO was much smoother and possessed fewer defects in the solidified charge. The relatively linear solidification characteristic leads to the generation of dense and small grains in the solidification process of BFFO.
4. The reduction in solidification defects also further improved the mechanical properties of BFFO, with significant improvements in compressive and tensile strength compared to DNTF, DNAN and TNT.

Due to the characteristics of high nitrogen content, low melting point, high energy density, low sensitivity, good thermal stability, few solidification defects and excellent comprehensive performance, BFFO has significant application potential as a melting cast explosive.

References

1. Ravi, P.; Badgujar, D.M.; Gore, G.M.; Tewari, S.P.; Sikder, A.K. Review on Melt Cast Explosives. *Propellants Explos. Pyrotech.* **2011**, *36*, 393–403. [CrossRef]
2. Szala, M.; Sabatini, J.J. 2,4,6-Trinitrotoluene—A Useful Starting Compound in the Synthesis of Modern Energetic Materials. *Z. Anorg. Allg. Chem.* **2018**, *644*, 262–269. [CrossRef]
3. Levine, B.S.; Furedi, E.M.; Gordon, D.E.; Barkley, J.J.; Lish, P.M. Toxic Interactions of the Munitions Compounds TNT and RDX in F344 Rats. *Toxicol. Sci.* **1990**, *15*, 373–380. [CrossRef]
4. Latendresse, C.; Fernandes, S.; You, S.; Euler, W. Speciation of the Products of and Establishing the Role of Water in the Reaction of TNT with Hydroxide and Amines: Structure, Kinetics, and Computational Results. *J. Phys. Chem. A* **2013**, *117*, 11167–11182. [CrossRef]
5. Yinon, J. *Toxicity and Metabolism of Explosives*; CRC Press: Boca Raton, FL, USA, 1990; pp. 38–39.
6. Esteve-Nunez, A.; Caballero, A.; Ramos, J.L. Biological Degradation of 2,4,6-Trinitrotoluene. *Microbiol. Mol. Biol. Rev.* **2001**, *65*, 335–352. [CrossRef]
7. Johnson, E.C.; Sabatini, J.J.; Chavez, D.E.; Sausa, R.C.; Byrd, E.F.; Wingard, L.A.; Guzmàn, P.E. Bis(1,2,4-oxadiazole)bis(methylene) Dinitrate: A High-Energy MeltCastable Explosive and Energetic Propellant Plasticizing Ingredient. *Org. Process Res. Dev.* **2018**, *22*, 736–740. [CrossRef]
8. Wang, Q.H. Overview of Carrier Explosive for Melt-Cast Composite Explosive. *Chin. J. Explos. Propellants* **2011**, *34*, 25–28.

9. Sinditskii, V.P.; Vu, M.C.; Sheremetev, A.B.; Alexandrova, N.S. Study on thermal decomposition and combustion of insensitive explosive 3,3′-diamino-4,4′-azofurazan (DAAzF). *Thermochim. Acta* **2008**, *473*, 25–31. [CrossRef]

10. Sheremetev, A.B.; Makhova, N.N.; Friedrichsen, W. Monocyclic furazans and furoxans. In *Advances in Heterocyclic Chemistry*; Academic Press: Cambridge, MA, USA, 2001; Volume 78, pp. 65–188.

11. Pepekin, V.I.; Korsunskii, B.L.; Matyushin, Y.N. Explosive properties of furoxanes. *Combust. Explos. Shock Waves* **2008**, *44*, 110–114. [CrossRef]

12. Bogdanova, Y.A.; Gubin, S.; Korsunskii, B.; Pepekin, V. Detonation characteristics of powerful insensitive explosives. *Combust. Explos. Shock Waves* **2009**, *45*, 738–743. [CrossRef]

13. Sheremetev, A. Nitro-and nitraminofurazans. *Ross Khim Zhurn* **1997**, *41*, 43–54.

14. Veauthier, J.M.; Chavez, D.E.; Tappan, B.C.; Parrish, D.A. Synthesis and Characterization of Furazan Energetics ADAAF and DOATF. *J. Energetic Mater.* **2010**, *28*, 229–249. [CrossRef]

15. Sinditskii, V.; Vu, M.; Burzhava, A.; Sheremetev, A.; Batog, L. Decomposition and combustion of 4, 4′-bis [4-aminofurazan-3-yl-azoxy]-3, 3′-azofurazan and its macrocyclic analog. In Proceedings of the 14th Seminar "New Trends in Research of Energetic Materials", Pardubice, Czech Republic, 13–15 April 2011; NTREM, University of Pardubice: Pardubice, Czech Republic, 2011; pp. 329–341.

16. Sheremetev, A.B.; Ivanova, E.A.; Spiridonova, N.; Melnikova, S.; Tselinsky, I.; Suponitsky, K.Y.; Antipin, M.Y. Desilylative nitration of C, N-disilylated 3-amino-4-methylfurazan. *J. Heterocycl. Chem.* **2005**, *42*, 1237–1242. [CrossRef]

17. Feng-Qi, Z.; Pei, C.; Rong-Zu, H.; Yang, L.; Zhi-Zhong, Z.; Yan-Shui, Z.; Xu-Wu, Y.; Yin, G.; Sheng-Li, G.; Qi-Zhen, S. Thermochemical properties and non-isothermal decomposition reaction kinetics of 3,4-dinitrofurazanfuroxan (DNTF). *J. Hazard. Mater.* **2004**, *113*, 67–71. [CrossRef]

18. Kotomin, A.A.; Kozlov, A.S.; Dushenok, S.A. Detonatability of high-energy-density heterocyclic compounds. *Russ. J. Phys. Chem. B* **2007**, *1*, 573–575. [CrossRef]

19. Zhou, Y.-S.; Zhang, Z.-Z.; Li, J.-K. Crystal structure of 3, 4-dinitrofurazanofuroxan. *Chin. J. Explos. Propellants* **2005**, *28*, 43.

20. Zhou, Y.; Xu, K.; Wang, B.; Zhang, H.; Qiu, Q.; Zhao, F. Synthesis, Structure and Thermal Properties of Bifurazano [3, 4-b: 3′, 4′-f] furoxano [3″, 4″-d] oxacyclohetpatriene (BFFO). *Bull. Korean Chem. Soc.* **2012**, *33*, 3317–3320. [CrossRef]

21. Stepanov, A.I.; Astrat'ev, A.A.; Dashko, D.V.; Spiridonova, N.P.; Mel'nikova, S.F.; Tselinskii, I.V. Synthesis of linear and cyclic compounds containing the 3,4-bis(furazan-3-yl)furoxan fragment. *Russ. Chem. Bull.* **2012**, *61*, 1024–1040. [CrossRef]

22. Stepanov, A.I.; Dashko, D.V.; Astrat'ev, A.A. Reduction of 7-R derivatives of 7H-tris[1,2,5]oxa-diazolo[3,4-b:3′,4′-d:3″,4″-f]azepine 1-oxide with furoxan ring opening. preparation of 4-R-4H-bis-[1,2,5]oxadiazolo[3,4-b:3′,4′-f]azepine-8,9-diamines. *Chem. Heterocycl. Compd.* **2013**, *49*, 1068–1081. [CrossRef]

23. Zhou, Y.S.; Wang, B.Z.; Wang, X.J.; Zhou, C.; Ning, Y.L.; Lian, P.; Li, J.K.; Zhang, G.Y. Synthesis and quantum chemistry study of novel bifurazano [3,4-b:3′,4′-f]furoxano[3″,4″-d]oxacyclohetpatriene. *Chin. J. Synth. Chem.* **2012**, *20*, 147–152.

24. Luo, Y.M.; Jiang, Q.L.; Zhao, K.; Wang, H. Analysis on differences of solidification behavior of DNAN and TNT. *Chin. J. Explos. Propellants* **2015**, *38*, 37–40. [CrossRef]

25. Luo, Y.M.; Zhao, K.; Jiang, Q.L.; Wang, H.; Wang, H.X. Difference analysis between solidification behavior of DNTF and TNT. *Hanneng Cailiao* **2016**, *24*, 74–78.

26. Chang, G.Q.; Wang, J.Z. *Crystal Growth and Control during Metal Solidification Process*; Metallurgical Industry Press: Beijing, China, 2002; p. 97.